Radiology

Diagnosis of Prostate Cancer with Noninvasive Estimation of Prostate Tissue Composition by Using Hybrid Multidimensional MR Imaging: A Feasibility Study[1]

Aritrick Chatterjee, PhD
Roger M. Bourne, PhD
Shiyang Wang, PhD
Ajit Devaraj, PhD
Alexander J. Gallan, MD
Tatjana Antic, MD
Gregory S. Karczmar, PhD
Aytekin Oto, MD

Purpose: To evaluate whether compartmental analysis by using hybrid multidimensional magnetic resonance (MR) imaging can be used to diagnose prostate cancer and determine its aggressiveness.

Materials and Methods: Twenty-two patients with prostate cancer underwent preoperative 3.0-T MR imaging. Axial images were obtained with hybrid multidimensional MR imaging by using all combinations of echo times (47, 75, 100 msec) and *b* values of 0, 750, 1500 sec/mm^2, resulting in a 3 × 3 array of data associated with each voxel. Volumes of the tissue components stroma, epithelium, and lumen were calculated by fitting the hybrid data to a three-compartment signal model, with distinct, paired apparent diffusion coefficient (ADC) and T2 values associated with each compartment. Volume fractions and conventional ADC and T2 were measured for regions of interest in sites of prostatectomy-verified malignancy (n = 28) and normal tissue (n = 71). Receiver operating characteristic (ROC) analysis was used to evaluate the performance of various parameters in differentiating prostate cancer from benign tissue.

Results: Compared with normal tissue, prostate cancer showed significantly increased fractional volumes of epithelium (23.2% ± 7.1 vs 48.8% ± 9.2, respectively) and reduced fractional volumes of lumen (26.4% ± 14.1 vs 14.0% ± 5.2) and stroma (50.5% ± 15.7 vs 37.2% ± 9.1) by using hybrid multidimensional MR imaging. The fractional volumes of tissue components show a significantly higher Spearman correlation coefficient with Gleason score (epithelium: ρ = 0.652, P = .0001; stroma: ρ = −0.439, P = .020; lumen: ρ = −0.390, P = .040) compared with traditional T2 values (ρ = −0.292, P = .132) and ADCs (ρ = −0.315, P = .102). The area under the ROC curve for differentiation of cancer from normal prostate was highest for fractional volume of epithelium (0.991), followed by fractional volumes of lumen (0.800) and stroma (0.789).

Conclusion: Fractional volumes of prostatic lumen, stroma, and epithelium change significantly when cancer is present. These parameters can be measured noninvasively by using hybrid multidimensional MR imaging and have the potential to improve the diagnosis of prostate cancer and determine its aggressiveness.

Online supplemental material is available for this article.

[1] From the Departments of Radiology (A.C., S.W., G.S.K., A.O.) and Pathology (A.J.G., T.A.), University of Chicago, 5841 S Maryland Ave, Chicago, IL 60637; Faculty of Health Sciences, University of Sydney, Sydney, Australia (R.M.B.); and Philips Research North America, Cambridge, Mass (A.D.). Received May 17, 2017; revision requested June 22; revision received October 9; accepted October 18; final version accepted November 14. **Address correspondence to** A.O. (e-mail: *aoto@radiology.bsd.uchicago.edu*).

Supported by the National Institutes of Health (grants NIH R01 CA172801 and NIH 1S10OD018448-01), Philips Healthcare, and the University of Chicago Medicine Comprehensive Cancer Center.

Prostate cancer is the most common noncutaneous cancer and second leading cause of death among men in the United States (1,2). Multiparametric magnetic resonance (MR) imaging is increasingly used in the detection, characterization, and staging of prostate cancer. Although MR imaging is very good at depicting the index lesion, a large number of prostate cancers go undetected due to their similarity to the normal gland and benign conditions (3,4). Therefore, histologic changes remain the reference standard for cancer detection. MR imaging microscopy of fixed prostate tissue with use of a preclinical 16.4-T MR unit has been used to image individual prostatic glands at sufficient resolution (40 μm isotropic) and demonstrated the different MR properties of gland microstructures and changes in these microstructures associated with cancer (5,6). However, the spatial resolution of clinical MR images is far too low to resolve glandular structures as prostate acini are approximately 0.1 mm in diameter (7).

Contrast on MR images is heavily dependent on tissue microstructure. However, most MR signal models are phenomenological models: monoexponential, biexponential, and kurtosis models. Although some model parameters (eg, apparent diffusion coefficients [ADCs] and T2 values) have been widely accepted for prostate cancer detection clinically, they provide little information regarding the underlying complex microstructure (8). More recently, structural models have been proposed. The Vascular, Extracellular, and Restricted Diffusion for Cytometry in Tumors, or VERDICT, model (9) characterizes diffusion in three distinct microstructural compartments and has the potential to characterize prostate cancer with good accuracy. However, the model uses increased cellularity as the primary marker for cancer. This is significantly different from histologic markers that are known to correlate with prostate cancer (10–13).

The reference standard for determining the aggressiveness of prostate cancer is the Gleason grading system, which is based on tissue architectural changes evaluated at histologic examination. In addition to these tissue architectural changes described by using the Gleason grading system, tissue composition in prostate cancer is different from that in normal prostate (10–12,14). A recent study showed that fractional volumes of the prostate gland components stroma, epithelium, and lumen correlate more strongly with cancer presence, Gleason grade, and ADC than "cellularity" metrics (10). There is increased epithelium and reduced lumen and stroma volume in cancers, and these changes increase with increasing Gleason grade. In addition, stroma, epithelium, and lumen have distinct diffusivities (5,6) and these diffusivities therefore might be used as a biomarker for noninvasive prostate cancer detection.

Current multiparametric models implicitly assume that the ADC and T2 are independent parameters. Thus, components with different ADCs may be identified from modeling diffusion data (5,6) and components with different T2 values may be identified from spin-echo measurements (15–18), but it is not known whether the different components identified with diffusion and T2 measurements have a direct one-to-one correspondence (8). Recent work demonstrated that the measured ADCs and T2 values are strongly interdependent and that this interdependence is different for different tissue compartments (19–21). Hybrid multidimensional MR imaging measures the change in ADC and T2 as a function of echo time and b value, respectively (17–19), and uses these changes as a source of information about the underlying tissue microstructure. As a result, hybrid multidimensional MR imaging could provide quantitative estimates of tissue composition by exploiting the coupled T2 and ADC values associated with each tissue component. Herein, we propose a model to estimate the volume fractions, ADCs, and T2 values of prostate stroma, epithelium, and lumen on the basis of their distinct, coupled diffusion and T2 relaxation properties. We performed this study to evaluate whether compartmental analysis with use of hybrid multidimensional MR imaging can potentially be used to diagnose prostate cancer and determine its aggressiveness.

Implication for Patient Care

- Prostate tissue composition estimated noninvasively by using hybrid multidimensional MR imaging has better diagnostic accuracy for detecting prostate cancer compared with T2 and apparent diffusion coefficient values.

Materials and Methods

Study Patients

This prospective study was conducted after institutional review board approval and was in compliance with the Health Insurance Portability and Accountability Act. Informed consent was obtained from all patients. Twenty-two consecutive patients (the first 22 who agreed to participate) with an elevated prostate-specific antigen level and biopsy-proven prostate cancer who were scheduled for radical prostatectomy were recruited

https://doi.org/10.1148/radiol.2018171130

Content codes: GU MR

Radiology 2018; 287:864–873

Abbreviations:
ADC = apparent diffusion coefficient
AFMS = anterior fibromuscular stroma
AUC = area under the ROC curve
ROC = receiver operating characteristic
ROI = region of interest

Author contributions:
Guarantors of integrity of entire study, A.C., A.O.; study concepts/study design or data acquisition or data analysis/interpretation, all authors; manuscript drafting or manuscript revision for important intellectual content, all authors; approval of final version of submitted manuscript, all authors; agrees to ensure any questions related to the work are appropriately resolved, all authors; literature research, A.C., R.M.B., S.W., A.D., G.S.K., A.O.; clinical studies, A.C., S.W., T.A., G.S.K., A.O.; experimental studies, A.C., R.M.B., S.W., A.D., A.J.G., G.S.K., A.O.; statistical analysis, A.C., S.W., A.D.; and manuscript editing, all authors

Conflicts of interest are listed at the end of this article.

for this study at our research center between March 2012 and December 2016. Among the exclusions for participation in the study was previous radiation or hormonal replacement therapy (which lead to alterations in prostatic signal intensity on MR images). Patients underwent imaging before prostatectomy. One patient was excluded due to an error in the imaging sequence, and that precluded compartmental analysis with hybrid multidimensional MR imaging. A provisional patent has been filed jointly by Philips Healthcare and the University of Chicago based on the prostate tissue composition estimation methodology described herein (22). Ten patients included in our current research were included in previous articles from our research group (20,21). The previous studies were pilot studies of hybrid multidimensional MR imaging that evaluated the changes in ADC and T2 as a function of echo time and *b* value, respectively, in prostate tissue. However, neither of those previous articles estimated tissue composition of prostate tissue noninvasively with use of compartmental analysis of hybrid multidimensional MR imaging data. The mean patient age was 65 years (range, 44–76 years), and the mean prostate-specific antigen level before MR imaging was 6.9 ng/mL (range, 2.3–18.9 ng/mL).

MR Imaging

Patients with previous histologically confirmed prostate cancer underwent preoperative multiparametric MR imaging with a 3.0-T MR unit (Achieva; Philips Healthcare, Best, the Netherlands) by using a six-channel cardiac phased-array coil placed around the pelvis combined with an endorectal coil (Medrad eCoil; Bayer Healthcare, Whippany, NJ). A 1-mg dose of glucagon (Glucagon; Eli Lilly & Co, Indianapolis, Ind) was injected to limit peristalsis of the rectal wall. The hybrid multidimensional MR imaging sequence consisted of a spin-echo module with diffusion sensitizing gradients placed symmetrically about the 180° pulse followed by single-shot echo-planar imaging readout. This pulse sequence was used to acquire images with echo times of 47, 75, and 100 msec. At each echo time, images were acquired with *b* values of 0, 750, and 1500 sec/mm^2, resulting in a 3 × 3 array of data associated with each image voxel. Hybrid multidimensional MR images were acquired in the axial plane and oriented perpendicular to the rectal wall, as guided by sagittal images. Fat saturation was performed by using spectrally adiabatic inversion recovery. The MR imaging parameters were as follows: repetition time = 3.5 seconds, in-plane resolution = 2.5 × 2.5 mm^2, imaging matrix = 72 × 72, field of view = 180 × 180 mm^2, section thickness = 3 mm, and reconstruction matrix = 128 × 128. The acquisition time was 12–15 minutes.

MR Image Analysis

The patients underwent radical prostatectomy. The prostate was fixed in formalin and serially sliced approximately in the same plane as MR images and cut into quadrants. Submitted tissue slices were embedded in paraffin, and hematoxylin-eosin–stained slides were made. The slides were evaluated for prostatic adenocarcinoma by an expert pathologist (T.A., with more than 10 years of experience). Areas of tumor were marked on the histologic slides. The quadrant sections were imaged by using a digital microscope and stitched together with Photoshop (Adobe Systems, San Jose, Calif) for correlation with MR images. The MR images were analyzed by an expert radiologist (A.O., with more than 10 years of experience with prostate MR imaging). Regions of interest (ROIs) were placed on ADC maps on sites of prostatectomy-verified malignancy (n = 28) and normal tissue (n = 71) from different prostate zones and propagated to maps of all parameters. The data collected were independent and no repeated measurements were taken as only one ROI from each distinct cancer lesion or one ROI representing normal tissue from each prostatic zone was taken for every patient. ROIs for cancer lesions smaller than 5 × 5 mm^2 were not marked and excluded from further analysis. T2 and ADC values were calculated by using a monoexponential signal decay model.

Tissue Component Volume

We modeled the MR signal from prostate tissue as unmixed pools of water in three tissue components: stroma, epithelium, and lumen. Tissue component volumes were calculated on a voxel-by-voxel basis by fitting the following equation with an in-house MATLAB program (MathWorks, Natick, Mass):

$$\begin{aligned}\frac{S}{S_0} = {} & V_{\text{stroma}} \exp\left(-\text{TE}/\text{T2}_{\text{stroma}}\right)\exp\left(-b \times \text{ADC}_{\text{stroma}}\right) \\ & + V_{\text{epithelium}} \exp\left(-\text{TE}/\text{T2}_{\text{epithelium}}\right) \\ & \exp\left(-b \times \text{ADC}_{\text{epithelium}}\right) \\ & + V_{\text{lumen}} \exp\left(-\text{TE}/\text{T2}_{\text{lumen}}\right) \\ & \exp\left(-b \times \text{ADC}_{\text{lumen}}\right),\end{aligned}$$

where V_{stroma}, $V_{\text{epithelium}}$, and V_{lumen} are the volume fractions of each compartment; $\text{T2}_{\text{stroma}}$, $\text{T2}_{\text{epithelium}}$, and T2_{lumen} the T2 values for each compartment; $\text{ADC}_{\text{stroma}}$, $\text{ADC}_{\text{epithelium}}$, and $\text{ADC}_{\text{lumen}}$ the ADCs for each compartment; S the signal intensity at each combination of echo time and *b* value; S_0 the signal intensity at the lowest echo time and *b* value; and TE the echo time. Detailed description of the constraints, assumptions, and thresholds chosen from previous literature values and with some input from the present data that were added to the surface-fitting program by using the nonlinear least squares method can be found in Appendix E1 (online).

The means ± standard deviations for ADC, T2, and the prostate tissue component volumes for stroma, epithelium, and lumen for each ROI were measured in MATLAB. A composite map to display all three tissue components in one image with use of volume fractions of stroma (green), epithelium (red), and lumen (blue) was produced.

Statistical Analysis

Statistical analysis was performed by using software (SPSS; IBM, Armonk, NY). A two-tailed *t* test was performed to assess the differences between means of calculated metrics from

cancer and normal prostate tissue. Because normal prostate tissue from different prostatic zones is histologically different and appears different on multiparametric MR images, normal tissue from different zones are treated differently for the subsequent analysis. The difference between means was assessed with one-way analysis of variance with the post hoc Tukey honest significant difference test. Only the analysis between cancer and normal tissue from different prostate zones was reported because the aim was to differentiate cancer from normal prostate tissue. The Spearman correlation coefficient (ρ) was calculated between Gleason score and calculated metrics. Receiver operating characteristic (ROC) analysis was used to evaluate the performance of the various parameters in differentiating cancer from normal prostatic tissue in different prostate zones. The area under the ROC curve (AUC) was reported. The Youden index from ROC analysis was used as a cutoff value to retrospectively predict the presence of prostate cancer.

Results

A total of 28 tumor ROIs (11 with Gleason grade 3+3, 11 with Gleason grade 3+4, three with Gleason grade 4+3, and three with Gleason grade 4+5) and 71 normal tissue ROIs (20 in peripheral zone, 19 in transition zone, 17 in central zone, and 15 in anterior fibromuscular stroma [AFMS]) were included in the analysis (Table 1). Figure 1 shows representative tissue composition maps for stroma, epithelium, and lumen estimated from hybrid multidimensional MR imaging and corresponding T2, ADC, and histologic maps with cancer sites marked. In the composite map of tissue composition, cancers appear red due to increased epithelium and loss of lumen and stromal volume (see example in Fig 1). Cancer was predicted as any voxel with a fractional volume of epithelium higher than 40% and fractional volumes of lumen less than 20% to compare with histologic images on the basis of the Youden index (Fig 1).

In cancer, the mean volume (±standard deviation) was significantly increased in epithelium and reduced in lumen and stroma compared with that in normal tissue (epithelium: 48.8% ± 9.2 vs 23.2% ± 7.1, respectively; lumen = 14.0% ± 5.2 vs 26.4% ± 14.1; stroma = 37.2% ± 9.1 vs 50.5% ± 15.7). In addition, ADC and T2 values were lower in cancer (ADC = 0.86 μm^2/msec ± 0.18, T2 = 76.3 msec ± 22.9) compared with normal prostate tissue (ADC = 1.34 μm^2/msec ± 0.24, T2 = 104.2 msec ± 47.1).

The fractional volumes of tissue components from compartmental analysis with hybrid multidimensional MR imaging and conventional ADC and T2 values are summarized in Table 2. The results of this study reflect the differences in histologic characteristics and conventional MR parameters (ADC and T2) between normal tissues from different prostate zones; therefore, the differentiation of cancer from normal prostate tissue in each prostate zone is different. Analysis of variance with the post hoc Tukey honest significant difference test found epithelial volume fraction was significantly higher (F = 73.337, $P = 7.6 \times 10^{-28}$) in cancer compared with normal tissue in all prostate zones. Luminal volume fraction was significantly lower (F = 41.798, $P = 4.3 \times 10^{-20}$) in cancer compared with normal tissue, except in AFMS, where no significant difference (P = .22) was found. Stromal volume fraction was significantly lower (F = 41.361, $P = 5.9 \times 10^{-20}$) in cancer compared with normal tissue in AFMS and transition zone but was not significantly different from normal tissue in peripheral and central zones. T2 values were significantly lower (F = 18.203, $P = 4.2 \times 10^{-11}$) in cancer compared with normal peripheral zone, but T2 values were not significantly different in cancer compared with normal transition zone and central zone tissue. In addition, T2 values in AFMS were lower than those in cancer. ADCs were significantly lower (F = 33.405, $P = 5.3 \times 10^{-21}$) in cancer compared with normal tissue from all prostate zones. Figure 2 shows box plots of ADC, T2 values, and estimated tissue compositions of stroma, epithelium, and lumen for cancer and normal tissue from different prostatic zones.

Table 1

Patient and Prostate Cancer Details

Parameter	Value
No. of patients	22
Mean age (y)*	65 (44–76)
Mean PSA level (ng/mL)*	6.9 (2.3–18.9)
Tumors marked	28
Gleason score	
3+3	11
3+4	11
4+3	3
4+5	3
Cancer location	
PZ	19
TZ	5
CZ	2
AFMS	2

Note.—Except where indicated, data are numbers of patients. AFMS = anterior fibromuscular stroma, CZ = central zone, PSA = prostate-specific antigen, PZ = peripheral zone, TZ = transition zone.

* Numbers in parentheses are the range.

The mean ADCs from the model fitting for the gland components stroma, epithelium, and lumen were 1.48 μm^2/msec ± 0.19, 0.43 μm^2/msec ± 0.15, and 2.81 μm^2/msec ± 0.13, respectively. The T2 values for stroma, epithelium, and lumen were 79.9 msec ± 22.9, 50.0 msec ± 17.4, and 664.9 msec ± 121.1, respectively. The average ADC and T2 values for each tissue component from cancer and normal tissue showed no significant differences (see Appendix E2 [online]).

Figure 3 shows the correlation of Gleason score with ADC, T2 values, and estimated tissue compositions of stroma, epithelium, and lumen. The fractional volumes of tissue components showed a significantly higher Spearman correlation coefficient with Gleason score (epithelium, ρ = 0.652, P = .0001; stroma, ρ = −0.439, P = .020; lumen, ρ = −0.390, P = .040), as compared with traditional T2 values (ρ = −0.292, P = .132) and ADCs (ρ = −0.315, P = .102) (Fig 3).

At ROC analysis, the AUC for differentiation of cancer from normal

Figure 1

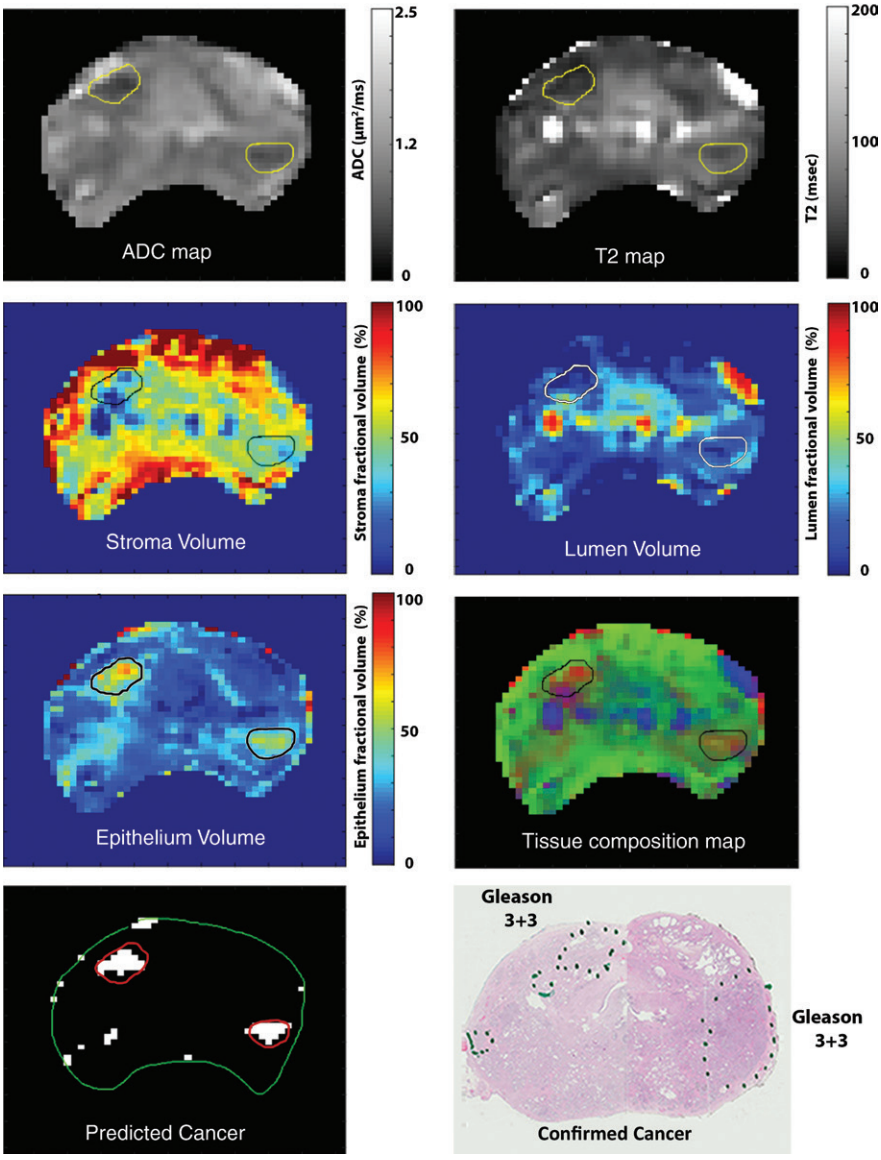

Figure 1: Tissue composition maps for stroma, epithelium, and lumen estimated by using hybrid multidimensional MR imaging and corresponding T2, apparent diffusion coefficient (*ADC*), and histologic maps with cancer sites marked (cancers had Gleason score of 3+3 in this case). Composite map displays all three tissue components in one image by using volume fractions of stroma (green), epithelium (red), and lumen (blue). Cancers appear red owing to increased epithelium and loss of lumen and stromal volume. Cancer was predicted as any voxel with fractional volume of epithelium higher than 40% and fractional volume of lumen less than 20%. Cancer 1 is in right transition zone (ADC = 0.93 μm^2/msec, T2 = 55.1 msec, volume fraction in stroma = 43.0%, volume fraction in epithelium = 46.4%, volume fraction in lumen = 10.6%). Cancer 2 is in left peripheral zone (ADC = 0.94 μm^2/msec, T2 = 73.9 msec, volume fraction in stroma = 42.5%, volume fraction in epithelium = 41.7%, volume fraction in lumen = 15.7%). Normal tissue from peripheral zone are not shown (ADC = 1.31 μm^2/msec, T2 = 87.4 msec, volume fraction in stroma = 51.5%, volume fraction in epithelium = 22.3%, volume fraction in lumen = 26.2%).

prostate in the entire prostate was found to be highest for fractional volume of epithelium (0.991), followed by fractional volume of lumen (0.800) and fractional volume of stroma (0.789). Detailed results from ROC analysis showing AUCs representing the diagnostic accuracy for detection of prostate cancer in each prostatic zone are shown in Table 3. The epithelium fractional volume showed the highest AUC in all prostate zones. Importantly, the combination of the three tissue components improves the diagnostic accuracy for prostate cancer detection, as evidenced by AUCs higher than independent measurements.

Discussion

The results of this study show that prostate tissue composition can be estimated noninvasively by using hybrid multidimensional MR imaging. The volume of epithelium is increased in cancer, whereas lumen and stroma volumes, along with ADC and T2 values, are decreased in cancer as compared with normal tissue. These trends and the values reported herein for cancer and normal tissue from different prostate zones are similar to those reported in the literature from morphometric analysis of tissue composition from hematoxylin-eosin–stained prostate tissue (10–12,16). Increasing Gleason score of prostate cancer showed correlation with increasing volume fraction of epithelium and reduced volume fractions of lumen and stroma. Prostate tissue composition determined by means of compartmental analysis of hybrid multidimensional MR imaging data were more strongly correlated with Gleason score than were conventional ADC and T2 values. Similarly, good correlation of tissue composition estimated in morphometric histologic studies with Gleason grading has been reported in the literature (10).

ROC analysis showed that increased epithelium and reduced lumen volume are very effective markers for the diagnosis of prostate cancer. The AUC for cancer detection was highest for epithelium volume fraction. In the

Table 2

Tissue Composition Estimates with Hybrid Multidimensional MR Imaging and Corresponding T2 and ADCs

Parameter	ADC (μm²/msec)	T2 (msec)	Volume Fraction (%)			No. of ROIs
			Stroma	Epithelium	Lumen	
Normal tissue	1.30 ± 0.23	104.2 ± 47.1	50.5 ± 15.7	23.2 ± 7.1	26.4 ± 14.1	71
Peripheral zone	1.49 ± 0.23	144.2 ± 59.3	39.0 ± 13.6	21.5 ± 4.6	39.4 ± 14.1	20
Transition zone	1.37 ± 0.19	103.8 ± 23.7	48.9 ± 7.8	23.2 ± 4.9	27.9 ± 7.4	19
Central zone	1.17 ± 0.10	98.6 ± 23.1	45.2 ± 7.1	29.7 ± 6.2	25.1 ± 5.5	17
AFMS	1.12 ± 0.15	57.6 ± 18.3	73.7 ± 7.0	17.9 ± 7.8	8.4 ± 5.6	15
Cancer tissue	0.86 ± 0.18	76.3 ± 22.9	37.2 ± 9.1	48.8 ± 9.2	14.0 ± 5.2	28
Gleason 6	0.90 ± 0.08	84.8 ± 14.2	41.1 ± 9.4	42.5 ± 5.4	16.4 ± 5.1	11
Gleason 7	0.89 ± 0.20	69.8 ± 26.2	36.3 ± 8.1	50.5 ± 7.5	13.2 ± 4.9	14
Gleason 9	0.61 ± 0.09	75.1 ± 30.1	27.4 ± 5.8	63.5 ± 7.7	9.1 ± 3.7	3
Spearman correlation (ρ) of Gleason score with calculated metrics*	−0.315 (−0.617, 0.133) [.102]	−0.292 (−0.658, 0.110) [.132]	−0.439 (−0.726, −0.062) [.020]	0.652 (0.322, 0.862) [.0001]	−0.390 (−0.663, −0.044) [.040]	…

Note.—Except where indicated, data are means ± standard deviations. ADC= apparent diffusion coefficient, AFMS = anterior fibromuscular stroma, ROIs = regions of interest.

* Numbers in parentheses are 95% confidence intervals of the correlation value. Numbers in brackets are *P* values.

peripheral zone (where most prostate cancer is located), the AUC for detecting cancer on the basis of epithelial and lumen volume fractions is higher than that for conventional T2 and ADC measurements reported in the literature (23,24). The transition zone is very heterogeneous, and benign prostatic hyperplasia in the transition zone can mimic prostate cancer on multiparametric MR images, making prostate cancer detection difficult (3). The present results suggest that cancers in the transition zone can be better detected with hybrid multidimensional MR imaging compared with conventional methods; hybrid multidimensional MR imaging helps detect reduced volume fractions of stroma and lumen and increased volume fraction of epithelium in cancers, and this yields higher AUCs than conventional ADC and T2 values reported in the literature (25,26). Central zone and AFMS cancers are difficult to diagnose because ADC and T2 values of normal tissue in these zones are low, similar to those of cancer (3,27). Our results suggest that increased epithelial volume fraction and decreased luminal volume fraction in central zone measured with hybrid multidimensional MR imaging are markers for cancer. In the AFMS, low stromal volume fraction and increased epithelial volume fraction can be indicative of prostate cancer. Although compartmental analysis of hybrid multidimensional MR imaging data in this study produced greater AUCs than ADC and T2 measurements, it should be noted that this comparison does not account for potential differences in signal-to-noise ratio. Hybrid multidimensional MR imaging data were collected over a longer acquisition period (12–15 minutes) compared with ADC and T2 data (3–7 minutes), and this could influence the comparison of AUCs.

The mean ADC and T2 values for stroma, epithelium, and lumen found in this study from the model fitting to hybrid multidimensional MR imaging data are close to values of ADC and T2 reported in the literature for tissue that is similar histologically to these three tissue compartments. The stromal ADC and T2 values are in the range of values reported for muscle (28) and similar to AFMS values. The lumen T2 is close to the value of the long T2 component reported from biexponential fitting of multiecho T2-weighted imaging of prostate tissue (15,16), and the luminal ADC is lower than that of pure water owing to the presence of proteins. It is difficult to identify a good model for pure epithelium as there is no prostatic region, even high-grade cancer, that is composed entirely of epithelium. The ADC calculated in this study for epithelium is lower than the lowest ADC measured for any single cancer ROI in our study and close to a reported ADC of 0.45 μm²/msec in an ex vivo study (5). In addition, the epithelium and stroma T2 values are close to values for the shorter T2 component reported from biexponential fitting of multiecho T2-weighted imaging of prostate tissue that is attributed to epithelial and stromal component (15,16).

Several previous studies have estimated tissue composition noninvasively to detect prostate cancer by modeling MR imaging data. The Vascular, Extracellular, and Restricted Diffusion for Cytometry in Tumors, or VERDICT, model enables differentiation of cancer from normal prostate tissue by estimating tissue cellularity with use of modified diffusion-weighted imaging sequences (9). However, it has been shown that changes in volume fractions of stroma, epithelium, and lumen estimated from histologic examination are a better predictor of prostate cancer than cellularity and show close correlation with Gleason grade (10). Another recent study showed that luminal volume estimated by using luminal water imaging could be used for detecting prostate cancer characterized by reduced luminal

Figure 2

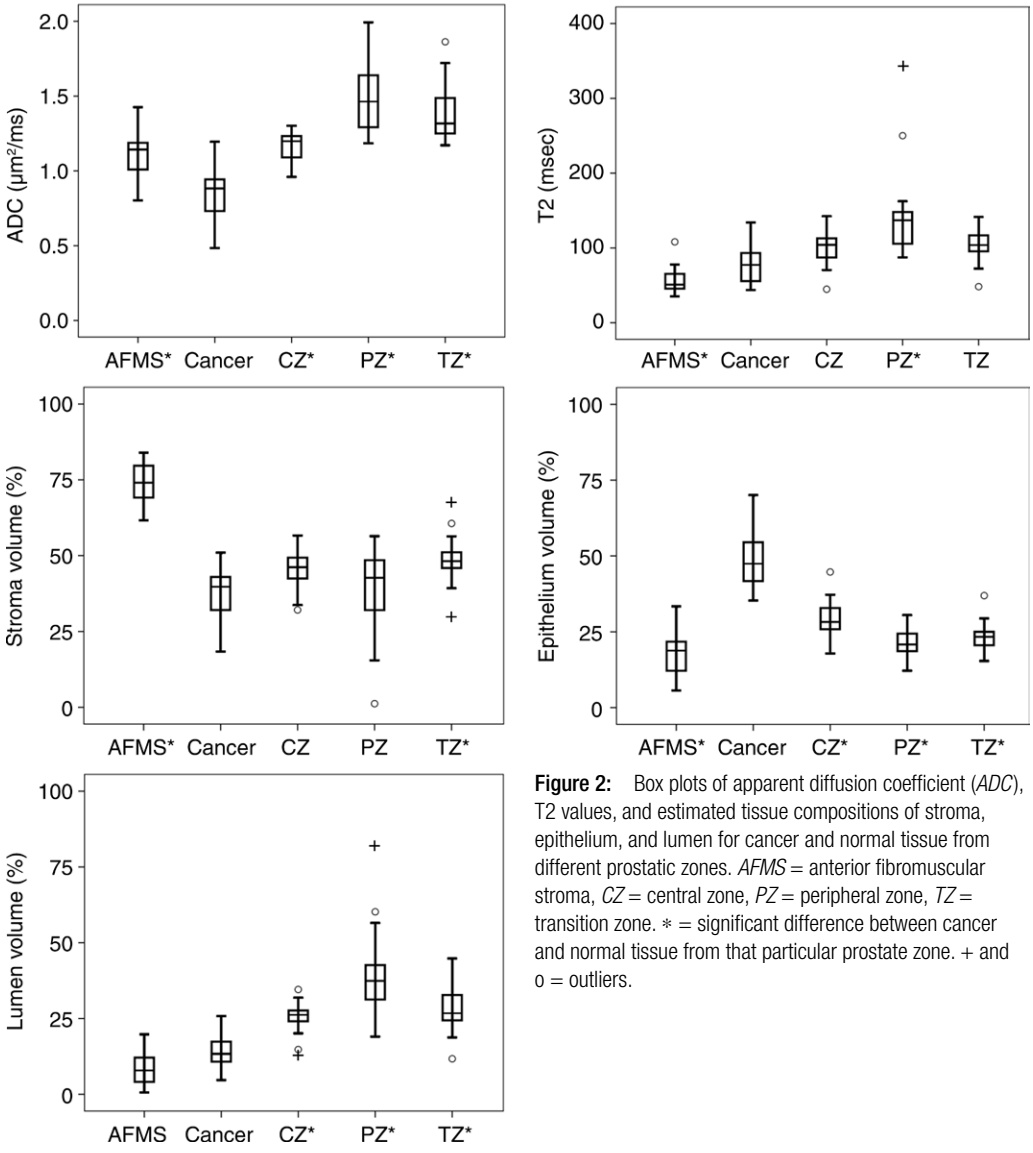

Figure 2: Box plots of apparent diffusion coefficient (*ADC*), T2 values, and estimated tissue compositions of stroma, epithelium, and lumen for cancer and normal tissue from different prostatic zones. *AFMS* = anterior fibromuscular stroma, *CZ* = central zone, *PZ* = peripheral zone, *TZ* = transition zone. * = significant difference between cancer and normal tissue from that particular prostate zone. + and o = outliers.

volume fraction compared with benign normal tissue (16,18). The drawback of the luminal water imaging model is highlighted by the low AUC for detecting anterior cancer (0.74)—especially in the AFMS, where benign tissue has a similar lumen volume to that of cancer. In addition, luminal water imaging may be unable to help separate the stromal and epithelium tissue compartments because they have similar T2 values, and this is crucial for cancer detection in the AFMS and transition zone. The results of our study show that stromal and epithelial compartments can be separated by using hybrid multidimensional MR imaging and anterior cancers can potentially be diagnosed more reliably. In addition, the AUC for prostate cancer diagnosis is improved by measuring both epithelium and stromal volume fractions instead of just the luminal volume fraction.

Our study had a number of limitations. Because of the absence of whole-mount histologic images for these cases, the volume estimates from our study were not compared with volumes derived from histologic examination. This is an important limitation of our study. This was an exploratory study to evaluate the feasibility of estimating prostate tissue components noninvasively with hybrid multidimensional MR imaging to aid in cancer detection. In the future, we plan on conducting a study correlating the volumes of stroma, epithelium, and lumen from hybrid multidimensional MR

Figure 3

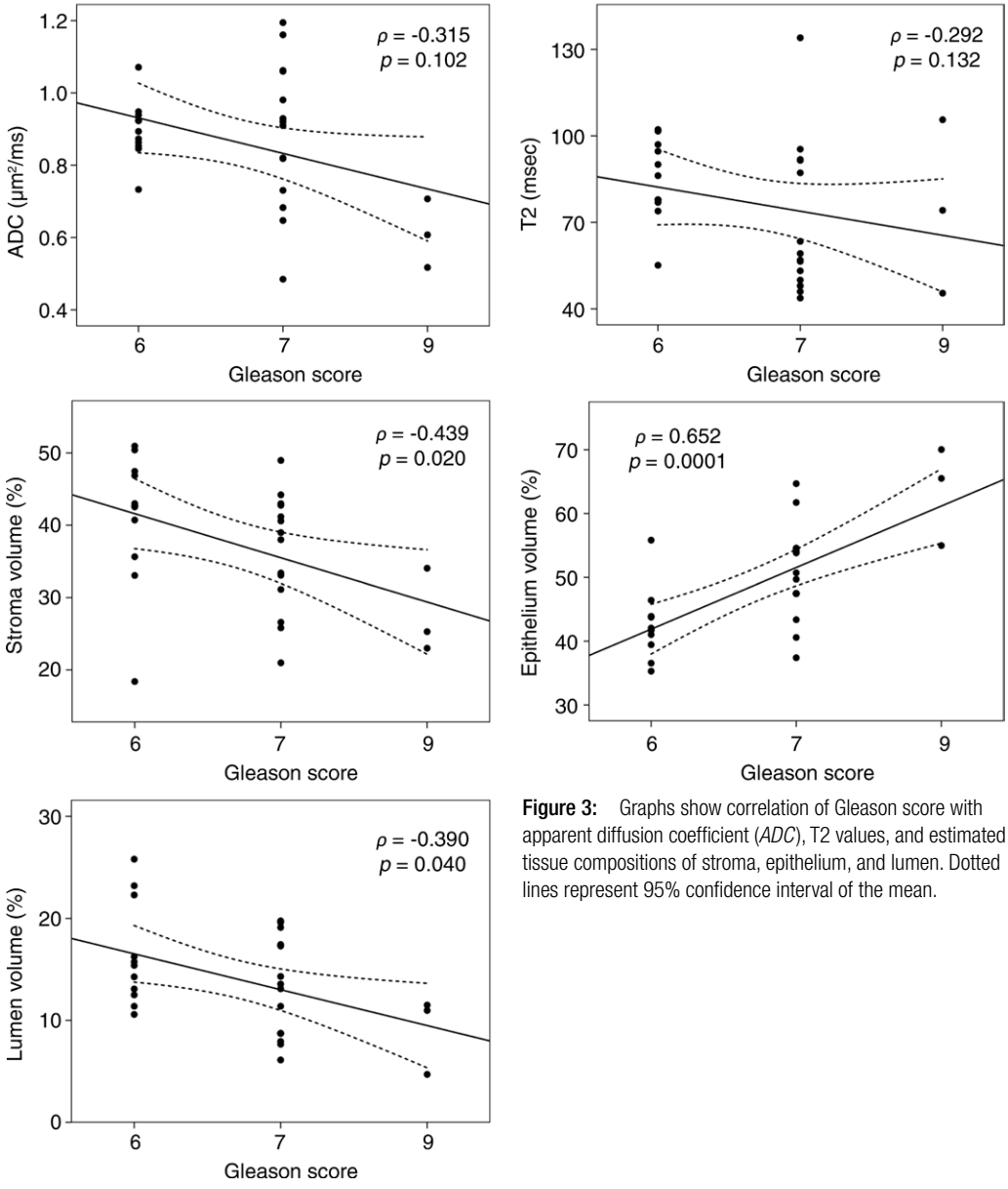

Figure 3: Graphs show correlation of Gleason score with apparent diffusion coefficient (*ADC*), T2 values, and estimated tissue compositions of stroma, epithelium, and lumen. Dotted lines represent 95% confidence interval of the mean.

imaging with ground truth results from hematoxylin-eosin–stained histologic slices. However, the tissue composition estimated noninvasively in this study by using hybrid multidimensional MR imaging is similar to the composition reported in the literature with morphometric analysis of hematoxylin-eosin–stained prostate tissue (10–12,16).

ROIs were drawn to define histologically confirmed cancer regions that were visible on MR images. Consequently, the histologic measures in these ROIs might be reflective of the dense region of the cancer rather than the whole cancer lesion. Sparse tumors have multiparametric MR imaging features, including ADC and T2, that are similar to those of benign prostatic tissue (29). Therefore, further study of both dense and sparse tumors is needed to properly evaluate the diagnostic accuracy of hybrid multidimensional MR imaging. In addition, tissue composition for benign features that mimic prostate cancer on multiparametric MR images, such as benign prostatic hyperplasia, prostatitis, atrophy, and calcification, were not analyzed separately in this study (3). Another study investigating the use of hybrid multidimensional MR imaging to characterize these conditions is needed.

Table 3

AUCs for Tissue Composition Estimates in Differentiating Cancer from Normal Prostate Tissue

Cancer Location	Volume Fraction in Stroma	Volume Fraction in Epithelium	Volume Fraction in Lumen	All Three Gland Components
Entire prostate	0.789 (0.699, 0.879) [8.0×10^{-6}]	0.991 (0.978, 1.000) [3.2×10^{-14}]	0.800 (0.715, 0.885) [4.0×10^{-6}]	0.994 (0.984, 1.000) [2.2×10^{-14}]
Peripheral zone	0.596 (0.423, 0.770) [.259]	1.000 (1.000, 1.000) [4.8×10^{-9}]	0.987 (0.963, 1.000) [1.1×10^{-8}]	1.000 (1.000, 1.000) [4.8×10^{-9}]
Transition zone	0.855 (0.742, 0.969) [4.2×10^{-5}]	0.996 (0.986, 1.000) [4.1×10^{-8}]	0.942 (0.870, 1.000) [3.5×10^{-7}]	1.000 (1.000, 1.000) [8.1×10^{-9}]
Central zone	0.754 (0.608, 0.900) [.005]	0.968 (0.916, 1.000) [1.8×10^{-7}]	0.922 (0.838, 1.000) [3.0×10^{-6}]	0.975 (0.931, 1.000) [1.2×10^{-7}]
AFMS	1.000 (1.000, 1.000) [8.7×10^{-8}]	1.000 (1.000, 1.000) [8.7×10^{-8}]	0.233 (0.075, 0.392) [.004]	1.000 (1.000, 1.000) [8.7×10^{-8}]

Note.—Data are areas under the receiver operating characteristic curve. Numbers in parentheses are confidence intervals. Numbers in brackets are *P* values. AFMS = anterior fibromuscular stroma.

In conclusion, in this study we showed that prostate tissue composition can be estimated noninvasively by using hybrid multidimensional MR imaging. The fractional volumes of prostatic lumen, stroma, and epithelium change significantly when cancer is present. The fractional volumes of the prostate tissue components stroma, epithelium, and lumen estimated noninvasively by using hybrid multidimensional MR imaging can be used for detecting prostate cancer and correlate more strongly with Gleason score than conventional T2 and ADC maps. The fractional volume of epithelium is higher and fractional volumes of lumen and stroma are lower in cancer compared with benign tissue. These novel quantitative parameters have the potential to improve the diagnosis of prostate cancer and determine its aggressiveness.

Disclosures of Conflicts of Interest: A.C. Activities related to the present article: received a grant from Philips Healthcare. Activities not related to the present article: disclosed no relevant relationships. Other relationships: has a patent pending. **R.M.B.** disclosed no relevant relationships. **S.W.** Activities related to the present article: received a grant from Philips Healthcare. Activities not related to the present article: disclosed no relevant relationships. Other relationships: disclosed no relevant relationships. **A.D.** Activities related to the present article: disclosed no relevant relationships. Activities not related to the present article: disclosed no relevant relationships. Other relationships: has a patent pending; is employed by Philips Research. **A.J.G.** disclosed no relevant relationships. **T.A.** disclosed no relevant relationships. **G.S.K.** Activities related to the present article: disclosed no relevant relationships. Activities not related to the present article: institution has a grant from Philips Healthcare. Other relationships: has a patent pending. **A.O.** Activities related to the present article: received a grant from Philips Healthcare. Activities not related to the present article: received grants from Guerbet Healthcare and Profound Healthcare; is on the medical advisory board at Profound Healthcare. Other relationships: has a patent pending.

References

1. Siegel R, Naishadham D, Jemal A. Cancer statistics, 2012. CA Cancer J Clin 2012;62(1):10–29.
2. Johnson LM, Choyke PL, Figg WD, Turkbey B. The role of MRI in prostate cancer active surveillance. BioMed Res Int 2014;2014:203906.
3. Kitzing YX, Prando A, Varol C, Karczmar GS, Maclean F, Oto A. Benign conditions that mimic prostate carcinoma: MR imaging features with histopathologic correlation. RadioGraphics 2016;36(1):162–175.
4. Rosenkrantz AB, Taneja SS. Radiologist, be aware: ten pitfalls that confound the interpretation of multiparametric prostate MRI. AJR Am J Roentgenol 2014;202(1):109–120.
5. Bourne RM, Kurniawan N, Cowin G, et al. Microscopic diffusivity compartmentation in formalin-fixed prostate tissue. Magn Reson Med 2012;68(2):614–620.
6. Bourne R, Kurniawan N, Cowin G, Sved P, Watson G. 16 T diffusion microimaging of fixed prostate tissue: preliminary findings. Magn Reson Med 2011;66(1):244–247.
7. Bourne R. Magnetic resonance microscopy of prostate tissue: how basic science can inform clinical imaging development. J Med Radiat Sci 2013;60(1):5–10.
8. Bourne R, Panagiotaki E. Limitations and prospects for diffusion-weighted MRI of the prostate. Diagnostics (Basel) 2016;6(2):21.
9. Panagiotaki E, Chan RW, Dikaios N, et al. Microstructural characterization of normal and malignant human prostate tissue with vascular, extracellular, and restricted diffusion for cytometry in tumours magnetic resonance imaging. Invest Radiol 2015;50(4):218–227.
10. Chatterjee A, Watson G, Myint E, Sved P, McEntee M, Bourne R. Changes in epithelium, stroma, and lumen space correlate more strongly with Gleason pattern and are stronger predictors of prostate ADC changes than cellularity metrics. Radiology 2015;277(3):751–762.
11. Langer DL, van der Kwast TH, Evans AJ, et al. Prostate tissue composition and MR measurements: investigating the relationships between ADC, T2, K(trans), v(e), and corresponding histologic features. Radiology 2010;255(2):485–494.
12. Kobus T, van der Laak JA, Maas MC, et al. Contribution of histopathologic tissue composition to quantitative MR spectroscopy and diffusion-weighted imaging of the prostate. Radiology 2016;278(3):801–811.
13. Selnæs KM, Vettukattil R, Bertilsson H, et al. Tissue microstructure is linked to MRI parameters and metabolite levels in prostate cancer. Front Oncol 2016;6:146.
14. Zhao M, Myint E, Watson G, Bourne R. Comparison of conventional histology and diffusion weighted microimaging for estimation of epithelial, stromal, and acinar volumes in prostate tissue [abstr]. In: Proceedings of the Twenty-First Meeting of the International Society for Magnetic Resonance in Medicine. Berkeley, Calif: International Society for Magnetic Resonance in Medicine, 2013; 3090.
15. Storås TH, Gjesdal KI, Gadmar ØB, Geitung JT, Kløw NE. Prostate magnetic resonance imaging: multiexponential T2 decay in prostate tissue. J Magn Reson Imaging 2008;28(5):1166–1172.
16. Sabouri S, Fazli L, Chang SD, et al. MR measurement of luminal water in prostate gland: quantitative correlation between MRI and histology. J Magn Reson Imaging 2017;46(3):861–869.
17. Kjaer L, Thomsen C, Iversen P, Henriksen O. In vivo estimation of relaxation processes in benign hyperplasia and carcinoma of the prostate gland by magnetic resonance imaging. Magn Reson Imaging 1987;5(1):23–30.

18. Sabouri S, Chang SD, Savdie R, et al. Luminal water imaging: a new MR imaging T2 mapping technique for prostate cancer diagnosis. Radiology 2017;284(2):451–459.

19. Does MD, Gore JC. Compartmental study of diffusion and relaxation measured in vivo in normal and ischemic rat brain and trigeminal nerve. Magn Reson Med 2000;43(6):837–844.

20. Wang S, Peng Y, Medved M, et al. Hybrid multidimensional T(2) and diffusion-weighted MRI for prostate cancer detection. J Magn Reson Imaging 2014;39(4):781–788.

21. Sadinski M, Karczmar G, Peng Y, et al. Pilot study of the use of hybrid multidimensional T2-weighted imaging-DWI for the diagnosis of prostate cancer and evaluation of Gleason score. AJR Am J Roentgenol 2016;207(3):592–598.

22. Devaraj A, Karczmar GS, Oto A, Chatterjee A. Non-invasive estimation of prostate tissue composition. US patent application 62563362. September 26, 2017.

23. Niaf E, Lartizien C, Bratan F, et al. Prostate focal peripheral zone lesions: characterization at multiparametric MR imaging—influence of a computer-aided diagnosis system. Radiology 2014;271(3):761–769.

24. Baur AD, Maxeiner A, Franiel T, et al. Evaluation of the prostate imaging reporting and data system for the detection of prostate cancer by the results of targeted biopsy of the prostate. Invest Radiol 2014;49(6):411–420.

25. Hoeks CM, Vos EK, Bomers JG, Barentsz JO, Hulsbergen-van de Kaa CA, Scheenen TW. Diffusion-weighted magnetic resonance imaging in the prostate transition zone: histopathological validation using magnetic resonance-guided biopsy specimens. Invest Radiol 2013;48(10):693–701.

26. Akin O, Sala E, Moskowitz CS, et al. Transition zone prostate cancers: features, detection, localization, and staging at endorectal MR imaging. Radiology 2006;239(3):784–792.

27. Ward E, Baad M, Peng Y, et al. Multiparametric MR imaging of the anterior fibromuscular stroma and its differentiation from prostate cancer. Abdom Radiol (NY) 2017;42(3):926–934.

28. Shiraishi T, Chikui T, Yoshiura K, Yuasa K. Evaluation of T2 values and apparent diffusion coefficient of the masseter muscle by clenching. Dentomaxillofac Radiol 2011;40(1):35–41.

29. Langer DL, van der Kwast TH, Evans AJ, et al. Intermixed normal tissue within prostate cancer: effect on MR imaging measurements of apparent diffusion coefficient and T2—sparse versus dense cancers. Radiology 2008;249(3):900–908.